

The CERN LHC Sensitivity on measuring $W^\pm Z\gamma$ Production and Anomalous $WWZ\gamma$ Coupling

Ke Ye, Daneng Yang, Qiang Li

*Department of Physics and State Key Laboratory of Nuclear Physics and Technology,
Peking University, Beijing, 100871, China*

E-mail: kevinye@pku.edu.cn, pmydn@pku.edu.cn, qliphy0@pku.edu.cn

ABSTRACT: In this paper we present for the first time a detailed Monte Carlo study of measuring $W^\pm Z\gamma$ production with pure leptonic decays and probing anomalous quartic gauge-boson $WWZ\gamma$ couplings at the $\sqrt{s} = 14$ TeV LHC, with parton shower and detector simulation effects taken into account. We find that with an integrated luminosity of 100 fb^{-1} and proper selection cuts, the Standard Model $W^\pm Z\gamma$ signal significance can be improved to as much as 3σ . After reviewing previous parametrization on anomalous $WWZ\gamma$ couplings (see e.g. a_n/Λ^2 or k_2^m/Λ^2 as shown in Ref. [17]), we propose a more general parametrization scheme with 4 free inputs leading only to genuine $WWZ\gamma$ aQGC couplings. Finally, our numerical results show that one can reach constraints at 95% confidence level of $-5.7 \times 10^{-5} \text{ GeV}^{-2} < k_2^m/\Lambda^2 < 5.5 \times 10^{-5} \text{ GeV}^{-2}$ and $-2.2 \times 10^{-5} \text{ GeV}^{-2} < a_n/\Lambda^2 < 2.4 \times 10^{-5} \text{ GeV}^{-2}$, which are more stringent than LEP's results by three orders of magnitude.

KEYWORDS: Triple Gauge Boson Production, Anomalous Quartic Gauge Boson Couplings, MC Simulation, LHC

Contents

1	Introduction	1
2	Effective Lagrangian for Photonic aQGCs	2
3	Event Simulation and Selection	4
4	Numerical Results	7
4.1	$W^\pm Z\gamma$ Production	7
4.2	Anomalous $WWZ\gamma$ Couplings	9
5	Conclusion and Discussion	12
A	Appendix: a more general parametrization to genuine $WWZ\gamma$ aQGCs	12

1 Introduction

The Standard Model (SM) has so far undergone considerable experimental tests and proved to be quite successful, especially after the recent discovery of the 125-126 GeV Higgs-like boson [1–4]. However, there are strong hints suggesting possible existence of new physics at or beyond TeV scale, arising from, e.g., the compelling astrophysical evidences on dark matter, and the large hierarchy between electroweak and Planck scale. Thus searching for new physics beyond the SM remains both a theoretical and experimental pursuit.

One possible way to explore new phenomena in particle physics is to investigate bosonic anomalous couplings. Under the framework of SM, $SU(2)_L \times U(1)_Y$ gauge symmetry completely determines gauge boson interactions, while presence of any anomalous coupling vertex may generate observable deviation from SM prediction. Study on these vector-boson interactions, therefore, can either confirm the SM and the spontaneously symmetry breaking mechanism, or give hint on the form of new physics.

So far, explorations of anomalous trilinear gauge boson couplings (aTGCs) have already been carried out extensively at the LEP [5, 6], Tevatron [7, 8], and later at the LHC [9, 10] via vector boson pair production, while less effort has been made on probing anomalous quartic gauge boson couplings (aQGCs). It is important to note that aQGCs, although involving more complicated event topology and may be less sensitive at high energy colliders, are not mere substitution of aTGCs but should be regarded as an independent way of uncovering new physics, since, for example, the exchange of heavy bosons can generate tree-level contribution to quartic coupling while its effect on trilinear vertex appears only at one-loop and is consequently suppressed [11, 12]. Historically, T. Han *et al.* in 1989 calculated the scattering cross sections of various triple gauge boson productions

at e^+e^- and later $p\bar{p}$ colliders [13, 14]. Monte Carlo (MC) studies were also performed later by Éboli *et al.* at $e\gamma$ colliders and $\gamma\gamma$ colliders through the processes $e\gamma \rightarrow VV'F$ ($V, V' = W, Z, \gamma$ and $F = e, \nu$) and $\gamma\gamma \rightarrow W^+W^-V$ ($V = Z, \gamma$), giving constraints on relevant aQGCs [15, 16]. Further MC work on aQGCs during that period were performed at e^+e^- collider, and can be found in *e.g.*, [17–20]. Direct constraints from experiments came mainly from the LEP at CERN, through $W^+W^- \gamma$ [21–23], $Z\gamma\gamma$ [24] and $\gamma\gamma\nu\bar{\nu}(q\bar{q})$ [25] channels. Due to limitations of center of mass energy, LEP’s constraints at 95% confidence level on anomalous coupling constant are approximately at 10^{-2} GeV^{-2} level, still two orders of magnitude larger than those from the oblique parameters S and U as argued in Ref. [26] ($1 \times 10^{-4} \text{ GeV}^{-2}$).

It is expected, comparatively, that the operation and its proposed upgrade within next few years of the Large Hadron Collider (LHC) at CERN will set more strict constraints on aQGCs. As shown in *e.g.*, [12, 26, 27], LHC can reach limits at about $10^{-5} - 10^{-6} \text{ GeV}^{-2}$ on the aQGCs, via the channel $W\gamma\gamma$, vector boson fusion (VBF) production of $\gamma\gamma$, $Z\gamma$ and WW . A more elaborated research by D. Yang *et al.* on $W^+W^- \gamma$ production with full leptonic decay also confirmed the potential of LHC on probing $WW\gamma\gamma$ aQGCs [28].

In the paper, we are interested in measuring $W^\pm Z\gamma$ final states with full leptonic decay at the $\sqrt{s} = 14 \text{ TeV}$ LHC and probing $WWZ\gamma$ anomalous coupling. This work extends our previous study on $W^+W^- \gamma$ and $WW\gamma\gamma$ aQGCs measurement [28] as a further independent examination on tripe gauge boson physics at the LHC. Moreover, we believe $W^\pm Z\gamma$ process has additional advantages as following: (1) $W^\pm Z\gamma$ process suffers from less background due to the requirement of a leptonically decayed Z -boson reconstructed; (2) Being sensitive to $WWZ\gamma$ vertex exclusively, $W^\pm Z\gamma$ serves as a direct examination on $WWZ\gamma$ aQGC.

Our paper is organized as follows. In Sec. 2 we describe the photonic aQGCs effective Lagrangian and a novel parametrization to genuine $WWZ\gamma$ aQGC. This is then followed by Sec. 3, showing our MC simulation framework and event selection details. Subsequently, Sec. 4 features numerical results, including the LHC sensitivities on $W^\pm Z\gamma$ production with pure leptonic decays and the $WWZ\gamma$ aQGC. Finally, we conclude in Sec. 5.

2 Effective Lagrangian for Photonic aQGCs

The quartic interaction can be constructed in a model-independent way with respect to the chiral Lagrangian approach [12, 17]. Assuming that new physics beyond the SM keeps $SU(2)_L \otimes U(1)_Y$ gauge invariance and $SU(2)_c$ custodial symmetry, we may write down the lowest order genuine aQGC $WWZ\gamma$ operators in the form of independent Lorentz structures [12, 17, 28]. We list below two previously commonly used expressions of $WWZ\gamma$ effective Lagrangian, both of which will be studied in this paper:

- (i) \mathcal{CP} -violating Lagrangian

$$\mathcal{L}_n = i \frac{\pi\alpha}{4\Lambda^2} a_n \epsilon_{ijk} W_{\mu\alpha}^{(i)} W_\nu^{(j)} W^{(k)\alpha} F^{\mu\nu}, \quad (2.1)$$

where α is the electroweak coupling constant, a_n characterizes the strength of anomalous coupling, Λ stands for new physics scale, $V_{\mu\nu}$ represents the field strength tensor given by

$\partial_\mu V_\nu - \partial_\nu V_\mu$, and $W_\mu^{(i)}$ is the $SU(2)$ weak isospin triplet:

$$\vec{W}_\mu^\rightarrow = \begin{pmatrix} \frac{1}{\sqrt{2}}(W^+ + W^-)_\mu \\ \frac{i}{\sqrt{2}}(W^+ - W^-)_\mu \\ W_\mu^3 - \frac{g'}{g}B_\mu \end{pmatrix}, \quad (2.2)$$

with θ_W symbolizing the Weinberg mixing angle. The expression was widely used in references, but Bélanger *et al.* [17] argued that it essentially violates \mathcal{CP} symmetry. However we emphasize that \mathcal{CP} invariance is not in general required by the first principle, thus we keep this form of effective Lagrangian for the purpose of comparison with previous experimental and MC outcomes [15, 18, 20–23].

- (ii) \mathcal{CP} -conserving Lagrangian

Following the notation in Ref. [12] (see Eq. (5) therein), there are 14 effective photonic operators relevant to aQGCs, specified by 14 independent coupling parameters $k_{0,c}^{w,b,m}$, $k_{1,2,3}^{w,m}$, $k_{1,2}^b$. After recombining and sorting various terms into similar Lorentz structures, one can see that among them five are related to anomalous $WWZ\gamma$ vertex:

$$\mathcal{W}_0^Z = -\frac{e^2 g^2}{\Lambda^2} F_{\mu\nu} Z^{\mu\nu} W^{+\alpha} W_\alpha^-, \quad (2.3)$$

$$\mathcal{W}_c^Z = -\frac{e^2 g^2}{2\Lambda^2} F_{\mu\nu} Z^{\mu\alpha} (W^{+\nu} W_\alpha^- + W^{-\nu} W_\alpha^+), \quad (2.4)$$

$$\mathcal{W}_1^Z = -\frac{e g_Z g^2}{2\Lambda^2} F^{\mu\nu} (W_{\mu\nu}^+ W_\alpha^- Z^\alpha + W_{\mu\nu}^- W_\alpha^+ Z^\alpha), \quad (2.5)$$

$$\mathcal{W}_2^Z = -\frac{e g_Z g^2}{2\Lambda^2} F^{\mu\nu} (W_{\mu\alpha}^+ W^{-\alpha} Z_\nu + W_{\mu\alpha}^- W^{+\alpha} Z_\nu), \quad (2.6)$$

$$\mathcal{W}_3^Z = -\frac{e g_Z g^2}{2\Lambda^2} F^{\mu\nu} (W_{\mu\alpha}^+ W_\nu^- Z^\alpha + W_{\mu\alpha}^- W_\nu^+ Z^\alpha), \quad (2.7)$$

where $g_Z = e/s_w c_w$, $g = e/s_w$, and we adopt the abbreviated symbol $c_w = \cos \theta_W$, $s_w = \sin \theta_W$.

Accordingly, the effective interactions can be expressed by the above operators as

$$\mathcal{L}_{eff} = \sum_i k_i^W \mathcal{W}_i^Z, \quad (2.8)$$

where the coefficient parameters k_i^W ($i = 0, c, 1, 2, 3$) can be written as

$$k_0^W = \frac{c_w}{s_w} k_0^w - \frac{s_w}{c_w} k_0^b + c_{zw} k_0^m, \quad (2.9)$$

$$k_c^W = \frac{c_w}{s_w} k_c^w - \frac{s_w}{c_w} k_c^b + c_{zw} k_c^m, \quad (2.10)$$

$$k_j^W = k_j^w + \frac{1}{2} k_j^m, \quad (j = 1, 2, 3), \quad (2.11)$$

as shown in [12]. Here $c_{zw} = (c_w^2 - s_w^2)/(2c_w s_w)$.

One would expect these k_i^W 's are correlated with those coupling constants that characterize $WW\gamma\gamma$, $ZZ\gamma\gamma$ and $ZZZ\gamma$ interactions [12]. A practicable way for decorrelation is to seek for proper subspace of these 14 parameters ($k_{0,c}^{w,b,m}$, $k_{1,2,3}^{w,m}$, $k_{1,2}^b$), namely, to impose extra restrictions on k_j^i , leaving only $WWZ\gamma$ vertex non-vanishing. A simple parametrization is proposed in Ref. [17], requiring $k_2^m = -k_3^m$ and others vanished, and then one has:

$$\mathcal{L}_{eff} = \frac{1}{2}k_2^m(\mathcal{W}_2^Z - \mathcal{W}_3^Z). \quad (2.12)$$

One alternative solution involving four independent parameters k_0^w , k_0^m , k_2^w , and k_2^m is given in Appendix. A, which can be expressed as:

$$k_0^W = \frac{1}{c_w s_w}(k_0^w + \frac{1}{2}k_0^m), \quad (2.13)$$

$$k_c^W = \frac{1}{c_w s_w}(k_0^w + \frac{1}{2}k_0^m), \quad (2.14)$$

$$k_1^W = -k_0^w - \frac{1}{2}k_0^m, \quad (2.15)$$

$$k_2^W = k_2^w + \frac{1}{2}k_2^m, \quad (2.16)$$

$$k_3^W = -(k_0^w + \frac{1}{2}k_0^m) - (k_2^w + \frac{1}{2}k_2^m). \quad (2.17)$$

The 4-dimensional solution automatically includes Eq. (2.12), if we set other three parameters than k_2^m to zero. In the following, we stick to this 4-dimensional parametrization, and in our analysis we first vary each parameter separately while setting others equal to zero, and then we also investigate the correlation of two individual parameters and draw contours at 95% confidence level.

Finally, we want to mention that, for sufficiently high energy collision, the effective Lagrangian leads to tree-level unitarity violation and is usually regulated by introducing appropriate form factor (ff) as following [12]:

$$k_2^m \rightarrow \frac{k_2^m}{(1 + \hat{s}/\Lambda_u^2)^n} \quad (2.18)$$

where \hat{s} is the the partonic center-of-mass energy and Λ_u represents the new physics scale. In Ref. [28] we see that a reasonable choice of form factor can indeed satisfy the unitarity requirement. In this paper we choose $n = 5$, $\Lambda_u = 2.5$ or ∞ TeV. The latter choice of Λ_u equals to no form factor at all.

3 Event Simulation and Selection

We carry out our MC simulations within MADGRAPH/MADEVENT v5 [29–31]. The effective Lagrangian of $WWZ\gamma$ aQGCs is implemented into MADGRAPH based on the FeynRules [32]-UFO [33]-ALOHA [34] framework. The signal and background concerned are initially generated at parton level by MADGRAPH and MADEVENT, and are then passed

through the interface to PYTHIA 6 for parton showering and hadronization [35]. The detector simulations are then done using DELPHES 2.0 [36] package, where we focus on the CMS detector at the LHC. Finally, all events are delivered to EXROOTANALYSIS [37] and analyzed with ROOT [38]. The work flow has also been used in our previous studies [28, 39].

The characteristic signal we are interested in contains three well-defined leptons with total electric charge ± 1 , in association with large missing transverse energy \cancel{E}_T . Besides, there is one and only one pair of oppositely charged lepton with same flavor originated from Z boson decay. Some example Feynman diagrams are plotted in Fig. 1, for $W^\pm Z\gamma$ production at the LHC, in the di-leptonic final state $l\nu L\bar{L}\gamma$, with $l, L = e, \mu$ and τ . Note τ decays into e, μ at the ratio of about 35% and is handled with TAUOLA [40].

In Fig. 1, two types of diagrams, Figs. 1(a) and 1(b), involve TGCs and are not sensitive to aQGCs, while Fig. 1(d) can also be seen as the initial and final state radiations (ISR and FSR) from the WZ production process, generated by PYTHIA. However, the ISR and FSR approximations in PYTHIA should break down for hard or wide scattering photon, e.g., when the transverse momentum of γ , $P_{T\gamma}$ is large. Note also this subset of contributions to $W^\pm Z\gamma$ is not related to QGCs, thus it would be interesting and important to show the overall $W^\pm Z\gamma$ results subtracting the contributions of the ISR/FSR approximations of Fig. 1(c), which we denote as pure_Vs:

$$\text{pure_Vs} \equiv W^\pm Z\gamma - W^\pm Z \text{ ISR/FSR.} \quad (3.1)$$

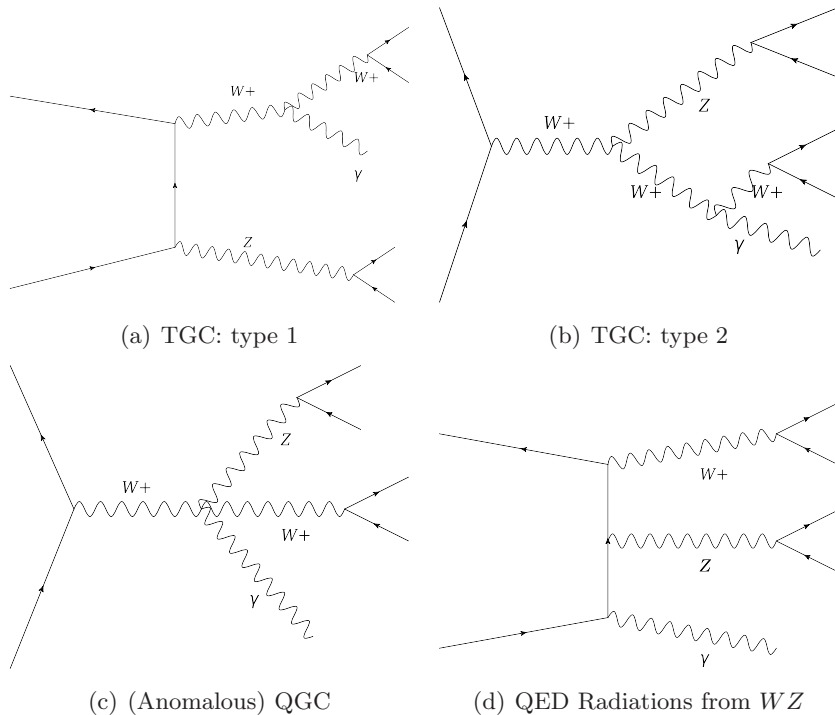


Figure 1. Sample Feynman diagrams that contribute to $W^\pm Z\gamma$ productions in $p p$ collision.

Aside from WZ ISR/FSR, another six backgrounds are taken into account: ZZ , $ZZ\gamma$, ZZZ , WWW , WWZ and $t\bar{t}Z$. Note that multi-lepton ($n > 3$) final state can be possible

backgrounds with additional leptons misidentified. Here we do not consider backgrounds with photons from jet fragmentation, in which the photons tend to be close to jets and the contributions can be suppressed efficiently via photon isolation cuts (see e.g. Ref. [41]).

We choose the following pre-selection cuts to generate unweighted events at parton level with MADGRAPH/MADEVENT to interface later with PYTHIA and DELPHES,

- (1) $P_{T,\gamma,l} \geq 15$ GeV,
- (2) $|\eta_\gamma| < 2.5, |\eta_l| < 2.5,$
- (3) $R_{ll} > 0.4, R_{l\gamma} > 0.4,$

where R denotes the separation $\sqrt{\Delta\phi^2 + \Delta\eta^2}$ in which ϕ being the azimuthal angle and η the pseudo-rapidity of a particle. Note, however, for the backgrounds involving misidentified leptons, we do not require any of the above cuts on leptons in order not to make bias.

Moreover, in the hard process generation with MADGRAPH/MADEVENT we adopt the CTEQ6L1 parton distribution functions (PDFs) [42] and set the renormalization and factorization scales as the transverse mass of the core process.

Further reconstruction cuts are then imposed on the reconstructed objects in the DELPHES settings cards,

- $P_{T,e,\mu,\gamma} \geq 15$ GeV, and $|\eta_{e,\mu,\gamma}| < 2.4.$
- Jets are clustered according to the anti- k_t algorithm with a cone radius $\Delta R = 0.5.$ Moreover, $P_{T,j} > P_{T,j}^{cut}$ (25 GeV by default) and $|\eta_j| < 5$ are required.

Tighter cuts are set in the analysis steps posterior to detector simulation,

- (1) The leading photon $P_{T,\gamma}$ should exceed the threshold, $P_{T,\gamma}^{cut}$, the value of which will be optimized,
- (2) $\cancel{E}_T > 40$ GeV,
- (3) To distinguish from background processes (e.g., $t\bar{t}Z$) with more hard jets, require $P_{T,j} < P_{T,j}^{veto}$ and at most 1 jet is allowed,
- (4) Three and only three leptons with ± 1 total charge,
- (5) Exclude b -tagged jets to suppress top quark-related production,
- (6) $R_{j\gamma}, R_{l\gamma}, R_{ll} > 0.5,$
- (7) One and only one pair of oppositely charged lepton with same flavor comes from Z boson decay, with $|m_{ll} - M_Z| < 10$ GeV.

In DELPHES, photons and charged leptons may overlap with the jet collections: DELPHES first reconstructs photons and leptons based on MC information, and then jets which can be seeded from the already reconstructed photons or leptons. In our analysis, we clean

the lepton collections from jets by requiring the DELPHES’s calculated “EhadOverEem” (the energy deposition in the Hadron Calorimeter over the one in the Electromagnetic Calorimeter) smaller than 1. Moreover, we remove any jet with $R_{j\gamma} < 0.001$ as it would be indeed most like a photon.

4 Numerical Results

4.1 $W^\pm Z\gamma$ Production

As a first step, we are interested in estimating the feasibility of observing triple gauge boson $W^\pm Z\gamma$ production at the LHC, before going into aQGCs. As mentioned before, we are also interested in comparing overall $W^\pm Z\gamma$ results with the ones subtracting ISR/FSR contributions from WZ processes (see Eq. (3.1)).

To optimize our results, we introduce further the following 3 requirements (similar as in our previous $W^+W^-\gamma$ study [28]), in addition to all the cuts as mentioned in Sec. 3: (A) Maximize sensitivities by varying photon P_T threshold cut $P_{T,\gamma}^{cut}$; (B) Keep the best $P_{T,\gamma}^{cut*}$, optimize over $P_{T,j}^{veto}$; (C) Keep the best $P_{T,\gamma}^{cut*}$ and $P_{T,j}^{veto*}$ values, vary $P_{T,j}$ threshold cut, and further require that within the interval $[P_{T,j}^{cut*}, P_{T,j}^{veto*}]$ at most 1 jet exists. The significance is defined by [43]

$$Q = \left(1 + \frac{N_s}{N_b}\right)^{N_{obs}} e^{-N_s}, \quad \text{significance} = \sqrt{2\ln Q}, \quad (4.1)$$

where N_s , N_b stand for number of signal and number of backgrounds, and $N_{obs} = N_s + N_b$.

We list the event numbers for the signal and backgrounds in Table 1, with the optimized parameters (optimized for pure_Vs contributions) from the above 3 steps: (A*) $P_{T,\gamma}^{cut*} = 80$ GeV, (B*) $P_{T,j}^{veto*} = 80$ GeV, (C*) $P_{T,j}^{cut*} = 35$ GeV. Related K-factors for the signal and backgrounds are also listed with references in Table 1. Correspondingly, the significances are shown in Fig. 2, calculated with Eq. (4.1).

Processes	σ (LO) [fb]	K-factor [Ref.]	Events		
			(A*) $P_{T,\gamma}^{cut*} = 80$ GeV	(B*) $P_{T,j}^{veto*} = 80$ GeV	(C*) $n_j = 0, 1, P_{T,j}^{cut*} = 35$ GeV
$W^\pm Z\gamma$	0.89	2.0 [44]	3.78	3.48	3.41
I(F)SR WZ	349.4	1.8 [45]	0.76	0.50	0.44
$ZZ\gamma$	0.24	1.4 [46]	0.19	0.18	0.17
ZZ	99.4	1.6 [45]	0.16	0.16	0.16
ZZZ	0.059	1.5 [47]	0.008	0.007	0.007
WWW	1.72	1.8 [47]	0	0	0
WWZ	0.96	1.9 [48]	0.085	0.079	0.073
$t\bar{t}Z$	6.16	1.4 [49]	0.35	0.16	0.086

Table 1. Cut flow at the LHC with $\sqrt{s} = 14$ TeV and integrated luminosity of 100 fb^{-1} .

More details can also be checked in Fig. 2 for cuts optimization. Note we also give the pure_Vs-curves to show the results after subtracting ISR/FSR contributions from WZ processes, as mentioned above. One can see that higher $P_{T,\gamma}^{cut}$ only slightly changes the $WZ\gamma$ significance as it removes both signal and backgrounds in a similar way, on the other hand, pure aQGCs pure_Vs-significance is enhanced quickly as more ISR/FSR background is killed. $P_{T,j}^{veto}$ cuts a bit more top-related backgrounds but the overall effects on significance is small. Increasing jet reconstructing cut $P_{T,j}^{cut}$, increases the 0-jet contributions while decreases the 1-jet ones, as expected. The overall 0+1 jet significances shrink slightly, as signal events are also discarded.

Above all, a significance about 3σ can be achieved to observe $WZ\gamma$ production at the 14 TeV LHC, and does not depend so much on the cuts as mentioned above. Note a large portion of $WZ\gamma$ events can come from the QED ISR/FSR WZ which is not related to QGCs, as shown by the pure_Vs-curves in Fig. 2, however, sticking to large $P_{T,\gamma}$ lower cut (~ 80 GeV), one can still get a total significance about 2σ from pure_Vs contributions.

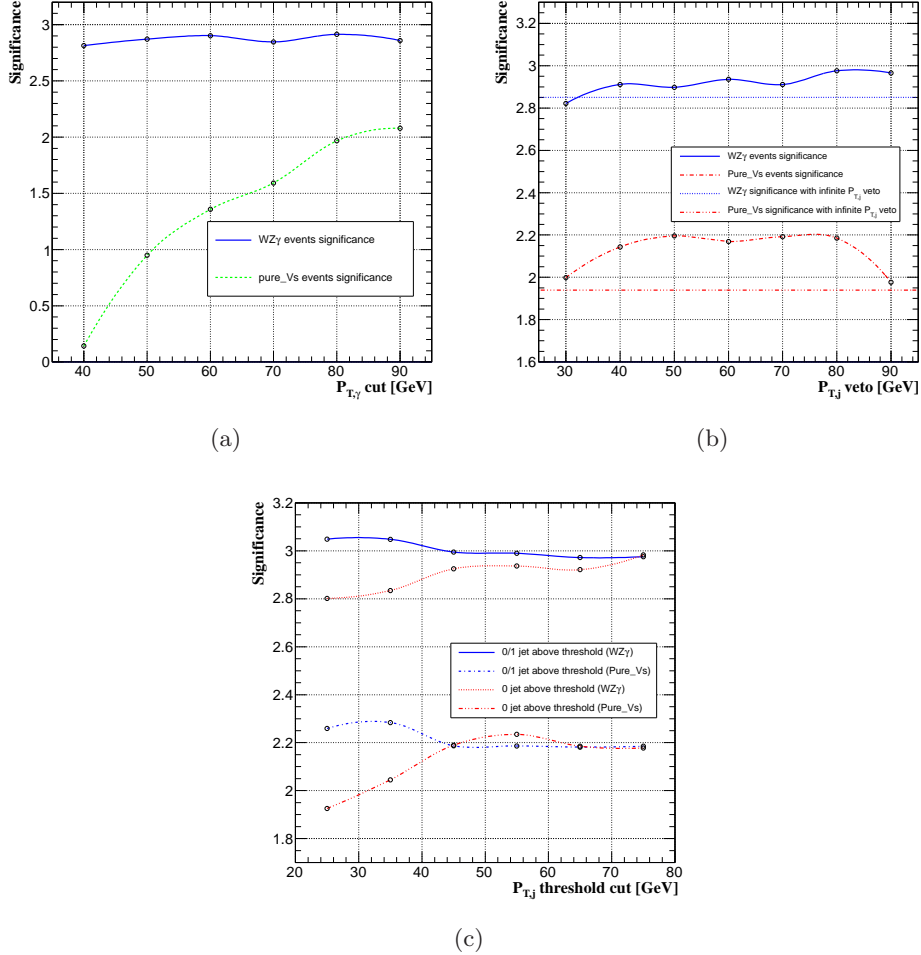


Figure 2. $W^\pm Z\gamma$ and pure_Vs significances, varying (a) $P_{T,\gamma}^{cut}$; (b) $P_{T,j}^{veto}$ in the presence of optimized $P_{T,\gamma}^{cut*}$; (c) $P_{T,j}^{cut}$ with optimized $P_{T,\gamma}^{cut*}$ and $P_{T,j}^{veto*}$.

4.2 Anomalous $WWZ\gamma$ Couplings

The $W^\pm Z\gamma$ signal process can be sensitive to aQGCs $WWZ\gamma$. As shown in Fig. 3, the aQGCs lead to excesses on the hard tails in various kinematic region. One thus can refine the cuts in Sec. 3 to enhance the sensitivity to aQGCs as following, e.g. :

- (1) $P_{T,\gamma} \geq 200$ GeV,
- (2) $P_{T,l} \geq 120$ GeV.

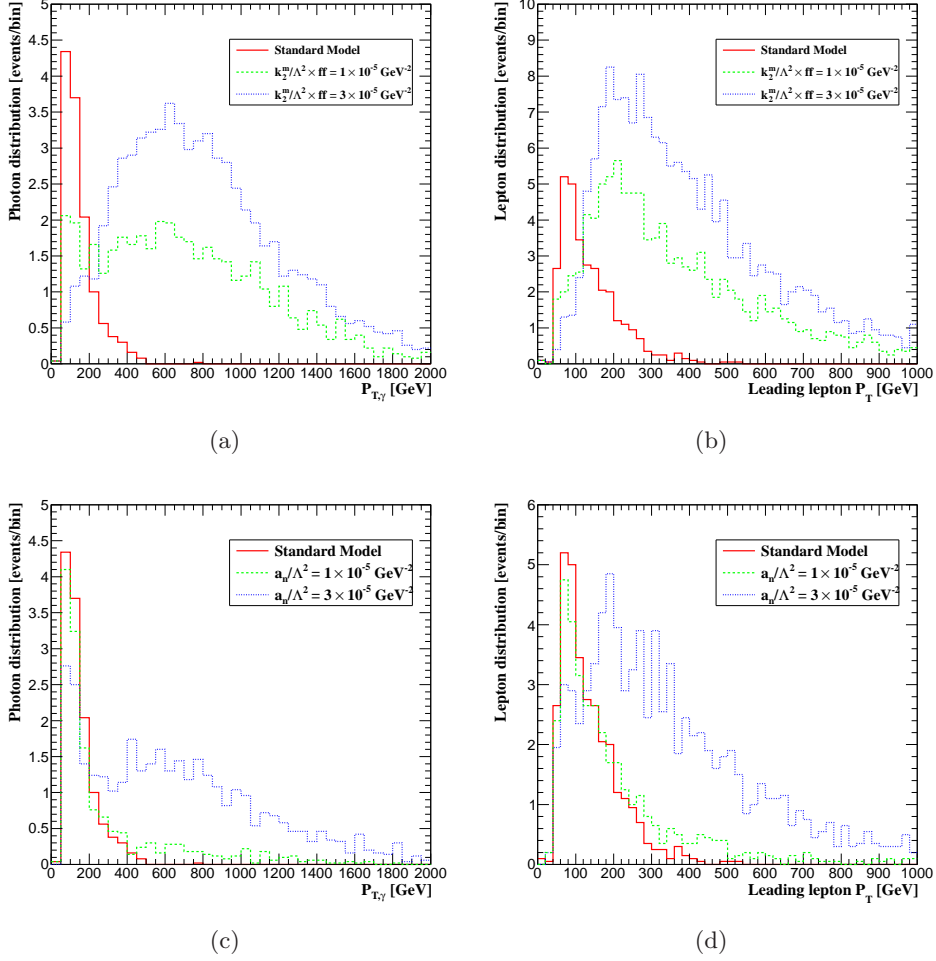


Figure 3. Comparisons of the differential distributions for $WZ\gamma$ productions at the LHC in leading lepton P_T and photon P_T , with $WWZ\gamma$ aQGCs following (a-b) \mathcal{CP} conserving Lagrangian (Eq. (2.12)); (c-d) \mathcal{CP} violating Lagrangian (Eq. (2.1)) without form factor.

After all these selection cuts, the significances are calculated and displayed in Fig. 4 as functions of the $WWZ\gamma$ aQGCs within \mathcal{CP} conserving Lagrangian (Eq. (2.12)) or \mathcal{CP} violating Lagrangian (Eq. (2.1)), at the 14 TeV LHC, with an integrated luminosity of 30, 100 and 200 fb^{-1} , respectively. The horizontal dash lines here correspond to the 95% confidence level limit. Note here the signal is defined as (QGCs – SM $WZ\gamma$).

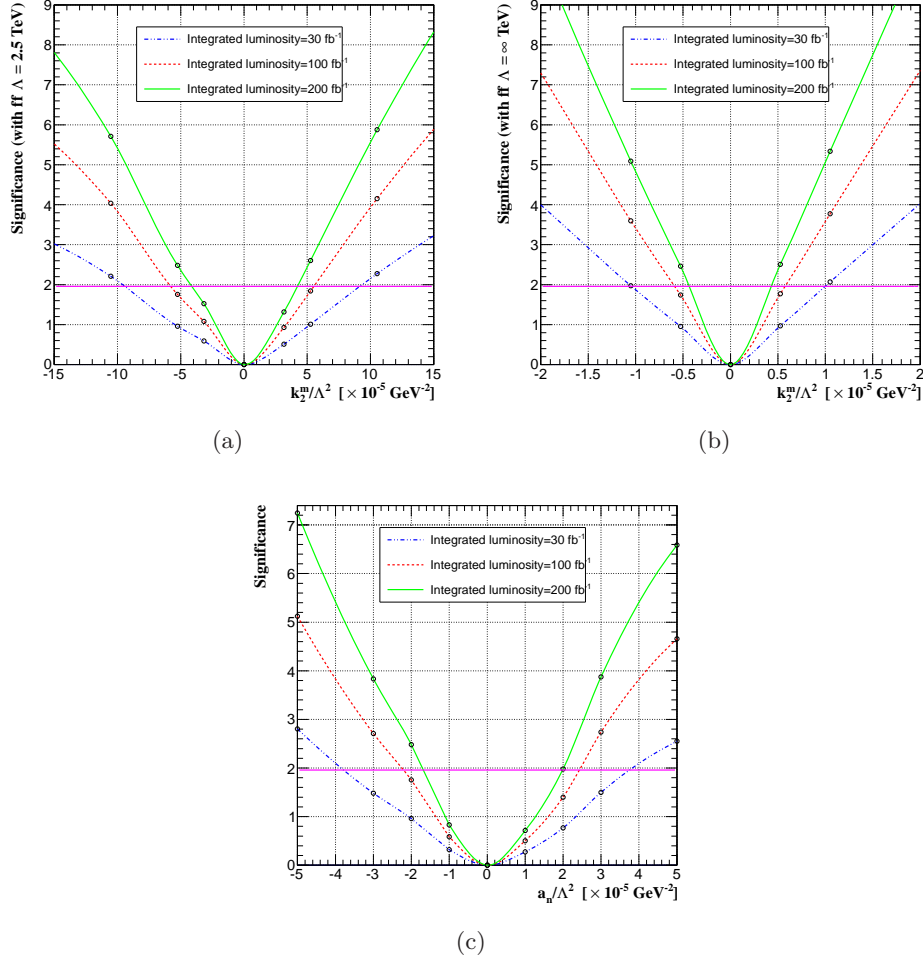


Figure 4. Anomalous coupling signal significance: (a) \mathcal{CP} conserving Lagrangian (Eq. (2.12)) with form factor $n=5$ and $\Lambda_u = 2.5$ TeV; (b) \mathcal{CP} conserving Lagrangian (Eq. (2.12)) with form factor $n=5$ and $\Lambda_u = \infty$ TeV; (c) \mathcal{CP} violating Lagrangian (Eq. (2.1)) without form factor.

Performing linear interpolation, 95% C.L. limits on $WWZ\gamma$ aQGCs are obtained (the constraints of k_2^m, k_0^w, k_0^m and k_2^w are derived assuming independence among them, *i.e.*, varying one parameter while setting others zero, with the parametrization given in Appendix. A) at the 14 TeV LHC, with an integrated luminosity of 30(100)[200] fb^{-1} , respectively:

- (1) $\Lambda_u = 2.5$ TeV
 - $-9.5(-5.7)[-4.1] \times 10^{-5} < k_2^m/\Lambda^2 < 9.2(5.5)[4.2] \times 10^{-5} \text{ GeV}^{-2}$,
 - $-2.6(-1.5)[-1.0] \times 10^{-5} < k_0^w/\Lambda^2 < 2.3(1.4)[0.9] \times 10^{-5} \text{ GeV}^{-2}$,
 - $-5.2(-3.0)[-2.0] \times 10^{-5} < k_0^m/\Lambda^2 < 4.6(2.8)[1.8] \times 10^{-5} \text{ GeV}^{-2}$,
 - $-4.8(-2.8)[-2.0] \times 10^{-5} < k_2^w/\Lambda^2 < 4.6(2.8)[2.1] \times 10^{-5} \text{ GeV}^{-2}$,
- (2) $\Lambda_u = \infty$ TeV:
 - $-1.0(-0.59)[-0.42] \times 10^{-5} < k_2^m/\Lambda^2 < 1.0(0.57)[0.41] \times 10^{-5} \text{ GeV}^{-2}$,

$$\begin{aligned}
& -1.7(-0.90)[-0.70] \times 10^{-6} < k_0^w/\Lambda^2 < 1.6(0.90)[0.60] \times 10^{-6} \text{ GeV}^{-2}, \\
& -3.4(-1.8)[-1.4] \times 10^{-6} < k_0^m/\Lambda^2 < 3.2(1.8)[1.2] \times 10^{-6} \text{ GeV}^{-2}, \\
& -0.50(-0.30)[-0.21] \times 10^{-5} < k_2^w/\Lambda^2 < 0.50(0.28)[0.20] \times 10^{-5} \text{ GeV}^{-2},
\end{aligned}$$

- (3) $-3.7(-2.2)[-1.7] \times 10^{-5} \text{ GeV}^{-2} < a_n/\Lambda^2 < 3.9(2.4)[2.0] \times 10^{-5} \text{ GeV}^{-2}$.

Fig. 5 illustrates the correlation between two coupling constants. The left subplot is for the case of k_2^w and k_2^m , as they always appear as the sum $k_2^w + \frac{1}{2}k_2^m$, the 2σ contour is simply band-like. The right subplot is for k_0^w and k_2^w , where the contour is more complex as a circle. Other correlations can be deduced from these two examples, for more details see Appendix A.

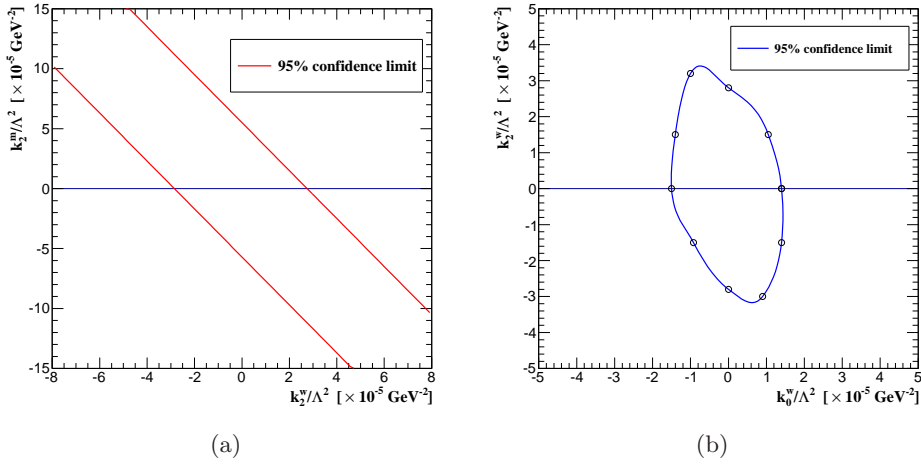


Figure 5. Correlations between anomalous coupling constants: 2σ contours for (a) k_2^w and k_2^m , and (b) k_0^w and k_2^w . Here we assume the \mathcal{CP} conserving Lagrangian with the form factor of $n=5$ and $\Lambda_u = 2.5 \text{ TeV}$, as well as the 14TeV LHC with 100 fb^{-1} of data.

Our results can be directly compared with the former experimental results and MC expectations. In Ref. [12] and [17], bounds on k_2^m/Λ^2 were derived through the MC simulations via VBF channel at the LHC and $e^+e^- \rightarrow W^+W^-\gamma, Z\gamma\gamma, ZZ\gamma$ processes, respectively. While in Ref. [21–23] (LEP experiments results) and [50] (MC expectations at $\gamma\gamma$ colliders), limits were given on a_n/Λ^2 . Summary of those results are listed in Table. 2 and Table. 3. At the 14 TeV LHC, we can set more stringent limit by at least three orders of magnitude compared to LEP results. Although a bit worse than the VBF channel, the leptonic decay mode of $W^\pm Z\gamma$ has simpler event topology and may be less contaminated by the QCD and VBF systematics.

parameter	95% confidence interval		
	$W^\pm Z\gamma$ ($\times 10^{-5}\text{GeV}^{-2}$)	MC VBF [12] ($\times 10^{-5}\text{GeV}^{-2}$)	MC at LEP2 [17] ($\times 10^{-2}\text{GeV}^{-2}$)
k_2^m/Λ^2	$[-5.7, 5.5]$	$[-2.7, 2.7]$	$[-6.2, 6.4]$

Table 2. Comparison of 95% C.L. limits on k_2^m/Λ^2 , between us and previous literatures [12, 17], with an integrated luminosity of 100 fb^{-1} at the 14 TeV LHC. The same form factor has been applied with $n = 5$ and $\Lambda_u = 2.5\text{ TeV}$ (Eq. (2.12)). Note the results from Ref. [12, 17] assume that all k_i^j s (Eq. (2.8)) are mutually independent, while we take the 4-dimensional parametrization as mentioned before in Sec. 2 which leads to genuine $WWZ\gamma$ aQGC but not e.g. $WW\gamma\gamma$ ones.

parameter	95% confidence interval				
	$W^\pm Z\gamma$ ($\times 10^{-5}\text{GeV}^{-2}$)	OPAL [21]	DELPHI [22]	L3 [23]	MC at $\gamma\gamma$ collider [50]
a_n/Λ^2	$[-2.2, 2.4]$	$[-0.61, 0.57]$	$[-0.18, 0.14]$	$[-0.41, 0.37]$	$[-0.03, 0.03]$

Table 3. Comparison of 95% C.L. limits on a_n/Λ^2 . The integrated luminosity of $W^\pm Z\gamma$ corresponds to 100 fb^{-1} at the 14 TeV LHC. For $\gamma\gamma$ collider simulations [50], the value relies on polarization of the beam and \sqrt{s} , and we pick the best value.

5 Conclusion and Discussion

The future upgrade of LHC with higher center of mass energy and luminosity enables measurement of triple gauge boson production and anomalous quartic gauge couplings, and $W^\pm Z\gamma$ production will be a potential channel which can be exploited to test the SM predictions and probe $WWZ\gamma$ anomalous coupling exclusively with lower background contamination.

In summary, our study shows that at the 14 TeV LHC with an integrated luminosity of 100 fb^{-1} , one can reach a significance of about 3σ to observe the SM $W^\pm Z\gamma$ production, and can constrain at 95% C.L. the anomalous $WWZ\gamma$ coupling parameters, e.g., k_2^m/Λ^2 and a_n/Λ^2 at $1 \times 10^{-5}\text{GeV}^{-2}$, respectively. The expected limits are far beyond the existing LEP results, and can be comparable with the ones from VBF MC simulation studies [12].

Acknowledgments

This work is supported in part by the National Natural Science Foundation of China, under Grants No. 10721063, No. 10975004, No. 10635030 and No. 11205008, and National Fund for Fostering Talents in Basic Science, under Grant No. J1103206.

A Appendix: a more general parametrization to genuine $WWZ\gamma$ aQGCs

Taking account all the coefficients that characterize each anomalous coupling, we have the following set of equations [12]:

$$k_i^\gamma = k_i^w + k_i^b + k_i^m, \quad i = 0, c, 1, \quad (\text{A.1})$$

$$k_{23}^\gamma = k_2^w + k_2^b + k_2^m + k_3^w + k_3^m \quad (\text{A.2})$$

$$k_0^Z = \frac{c_w}{s_w}(k_0^w + k_1^w) - \frac{s_w}{c_w}(k_0^b + k_1^b) + c_{zw}(k_0^m + k_1^m) \quad (\text{A.3})$$

$$k_c^Z = \frac{c_w}{s_w}(k_c^w + k_2^w + k_3^w) - \frac{s_w}{c_w}(k_c^b + k_2^b) + c_{zw}(k_c^m + k_2^m + k_3^m) \quad (\text{A.4})$$

$$k_0^W = \frac{c_w}{s_w}k_0^w - \frac{s_w}{c_w}k_0^b + c_{zw}k_0^m \quad (\text{A.5})$$

$$k_c^W = \frac{c_w}{s_w}k_c^w - \frac{s_w}{c_w}k_c^b + c_{zw}k_c^m \quad (\text{A.6})$$

$$k_j^W = k_j^w + \frac{1}{2}k_j^m, \quad (i = 1, 2, 3). \quad (\text{A.7})$$

Here the first four set of equations, (A.1) - (A.4), are the coupling constants of $WW\gamma\gamma$, $ZZ\gamma\gamma$, $ZZZ\gamma$ and thus are irrelevant to $WWZ\gamma$ coupling, and we would like to find a solution for which they vanish. Here we seek for restrictions on these parameters that can lead to zero of Eqs. (A.1) - (A.4), which are:

$$k_1^b = 0, \quad k_2^b = 0, \quad (\text{A.8})$$

$$k_0^w = k_c^w, \quad k_0^m = k_c^m, \quad k_0^b = k_c^b, \quad (\text{A.9})$$

$$k_1^m = k_2^m + k_3^m, \quad k_1^w = k_2^w + k_3^w, \quad (\text{A.10})$$

$$k_0^w + k_0^b + k_0^m = 0, \quad (\text{A.11})$$

$$\frac{c_w}{s_w}(k_0^w + k_1^w) - \frac{s_w}{c_w}(k_0^b + k_1^b) + c_{zw}(k_0^m + k_1^m) = 0, \quad (\text{A.12})$$

$$k_1^w + k_1^m = 0. \quad (\text{A.13})$$

The conditions Eqs.(A.11-A.13), lead to $2k_0^w + k_0^m + k_1^w = 0$. We have here in total 10 independent restrictions, hence leaving 4 independent variables. And we choose them to be k_0^w, k_0^m, k_2^w , and k_2^m . It is then easy to verify that the couplings constants can be expressed exactly as those in Eq. (2.13) - Eq. (2.17).

Having obtained the parameterization of genuine $WWZ\gamma$ aQGC, we may further investigate the correlations between two parameters while setting the remaining two zero, which involve a total of six combinations. We take the following two combinations as examples, and the other cases can be inferred in a similar manner:

- (1) $k_2^m, k_2^w \neq 0$.

It is easy to verify that we have $k_0^W = 0, k_c^W = 0, k_1^W = 0$ and $k_2^W = k_2^w + \frac{1}{2}k_2^m, k_3^W = -(k_2^w + \frac{1}{2}k_2^m)$. Observe that this special case is equivalent to Eq. (2.12), if we substitute k_2^m in (2.12) with $2k_2^w + k_2^m$. Thus restrictions on k_2^m and k_2^w can be expressed as (for 100 fb⁻¹ LHC and with $\sqrt{s} = 5$, for instance):

$$-5.7 \times 10^{-5} < (2k_2^w + k_2^m)/\Lambda^2 < 5.5 \times 10^{-5} \text{GeV}^{-2}. \quad (\text{A.14})$$

One may as well check that when only k_0^m and k_0^w are left non-zero, the confidence region can be extracted directly if we make substitution $k_0^w \rightarrow k_0^w + \frac{1}{2}k_0^m$ in the inequalities given in Sec. 4.2.

- (2) $k_0^w, k_2^w \neq 0$.

In fact we will see this is the only case we need to consider, where each coefficient k_i^W is written as:

$$k_0^W = \frac{1}{c_w s_w} k_0^w, \quad (\text{A.15})$$

$$k_c^W = \frac{1}{c_w s_w} k_0^w, \quad (\text{A.16})$$

$$k_1^W = -k_0^w, \quad (\text{A.17})$$

$$k_2^W = k_2^w, \quad (\text{A.18})$$

$$k_3^W = -k_0^w - k_2^w. \quad (\text{A.19})$$

Other cases can be related to above with simple substitutions. For example, when $k_0^m, k_2^m \neq 0$, one just needs to rewrite Eq.(A.15) - (A.19) with $k_0^w \rightarrow \frac{1}{2}k_0^m, k_2^w \rightarrow \frac{1}{2}k_2^m$.

References

- [1] F. Gianotti, CERN Seminar, Update on the Standard Model Higgs searches in ATLAS, July, 4 2012. ATLAS-CONF-2012-093
- [2] J. Incandela, CERN Seminar, Update on the Standard Model Higgs searches in CMS, July, 4 2012.
- [3] S. Chatrchyan *et al.* [CMS Collaboration], Phys. Lett. B **716**, 30 (2012) [arXiv:1207.7235 [hep-ex]].
- [4] G. Aad *et al.* [ATLAS Collaboration], Phys. Lett. B **716**, 1 (2012) [arXiv:1207.7214 [hep-ex]].
- [5] P. Achard *et al.* [L3 Collaboration], Phys. Lett. B **547**, 151 (2002) [hep-ex/0209015].
- [6] P. Abreu *et al.* [DELPHI Collaboration], Phys. Lett. B **502**, 9 (2001) [hep-ex/0102041].
- [7] K. Gounder [CDF and D0 Collaborations], hep-ex/9903038.
- [8] B. Abbott *et al.* [D0 Collaboration], Phys. Rev. D **62**, 052005 (2000) [hep-ex/9912033].
- [9] G. Aad *et al.* [ATLAS Collaboration], Phys. Rev. Lett. **108**, 041804 (2012) [arXiv:1110.5016 [hep-ex]].
- [10] S. Chatrchyan *et al.* [CMS Collaboration], Eur. Phys. J. C **73**, 2283 (2013) [arXiv:1210.7544 [hep-ex]].
- [11] G. Belanger and F. Boudjema, Phys. Lett. B **288**, 201 (1992).
- [12] O. J. P. Eboli, M. C. Gonzalez-Garcia and S. M. Lietti, Phys. Rev. D **69**, 095005 (2004) [hep-ph/0310141].
- [13] V. D. Barger, T. Han and R. J. N. Phillips, Phys. Rev. D **39**, 146 (1989).
- [14] T. Han and R. Sobey, Phys. Rev. D **52**, 6302 (1995) [hep-ph/9507409].
- [15] O. J. P. Eboli, M. C. Gonzalez-Garcia and S. F. Novaes, Nucl. Phys. B **411**, 381 (1994) [hep-ph/9306306].
- [16] O. J. P. Eboli, M. B. Magro, P. G. Mercadante and S. F. Novaes, Phys. Rev. D **52**, 15 (1995) [hep-ph/9503432].

- [17] G. Belanger, F. Boudjema, Y. Kurihara, D. Perret-Gallix and A. Semenov, *Eur. Phys. J. C* **13**, 283 (2000) [hep-ph/9908254].
- [18] W. J. Stirling and A. Werthenbach, *Eur. Phys. J. C* **14**, 103 (2000) [hep-ph/9903315].
- [19] S. Dawson, A. Likhoded, G. Valencia and O. Yushchenko, *eConf C* **960625**, NEW147 (1996) [hep-ph/9610299].
- [20] A. Denner, S. Dittmaier, M. Roth and D. Wackerroth, *Eur. Phys. J. C* **20**, 201 (2001) [hep-ph/0104057].
- [21] G. Abbiendi *et al.* [OPAL Collaboration], *Phys. Lett. B* **471**, 293 (1999) [hep-ex/9910069].
- [22] J. Abdallah *et al.* [DELPHI Collaboration], *Eur. Phys. J. C* **31**, 139 (2003) [hep-ex/0311004].
- [23] M. Acciarri *et al.* [L3 Collaboration], *Phys. Lett. B* **490**, 187 (2000) [hep-ex/0008022].
- [24] M. Acciarri *et al.* [L3 Collaboration], *Phys. Lett. B* **478**, 39 (2000) [hep-ex/0002037].
- [25] G. Abbiendi *et al.* [OPAL Collaboration], *Phys. Rev. D* **70**, 032005 (2004) [hep-ex/0402021].
- [26] O. J. P. Eboli, M. C. Gonzalez-Garcia, S. M. Lietti and S. F. Novaes, *Phys. Rev. D* **63**, 075008 (2001) [hep-ph/0009262].
- [27] C. Royon, E. Chapon and O. Kepka, *PoS DIS* **2010**, 089 (2010) [AIP Conf. Proc. **1350**, 140 (2011)] [arXiv:1008.0258 [hep-ph]].
- [28] D. Yang, Y. Mao, Q. Li, S. Liu, Z. Xu and K. Ye, *JHEP* **1304**, 108 (2013) [arXiv:1211.1641 [hep-ph]].
- [29] J. Alwall *et al.*, *JHEP* **0709**, 028 (2007) [arXiv:0706.2334 [hep-ph]].
- [30] J. Alwall, M. Herquet, F. Maltoni, O. Mattelaer and T. Stelzer, *JHEP* **1106** (2011) 128 [arXiv:1106.0522 [hep-ph]].
- [31] F. Maltoni and T. Stelzer, *JHEP* **0302**, 027 (2003) [hep-ph/0208156].
- [32] N. D. Christensen and C. Duhr, *Comput. Phys. Commun.* **180**, 1614 (2009) [arXiv:0806.4194 [hep-ph]].
- [33] C. Degrande, C. Duhr, B. Fuks, D. Grellscheid, O. Mattelaer and T. Reiter, *Comput. Phys. Commun.* **183**, 1201 (2012) [arXiv:1108.2040 [hep-ph]].
- [34] P. de Aquino, W. Link, F. Maltoni, O. Mattelaer and T. Stelzer, arXiv:1108.2041 [hep-ph].
- [35] T. Sjostrand, L. Lonnblad, S. Mrenna and P. Z. Skands, hep-ph/0308153.
- [36] S. Ovin, X. Rouby and V. Lemaitre, arXiv:0903.2225 [hep-ph].
- [37] <http://madgraph.hep.uiuc.edu/Downloads/ExRootAnalysis>
- [38] R. Brun and F. Rademakers, *Nucl. Instrum. Meth. A* **389**, 81 (1997).
- [39] S. Liu, Y. Mao, Y. Ban, P. Govoni, Q. Li, C. Asawatangtrakuldee and Z. Xu, *Phys. Rev. D* **86**, 074010 (2012) arXiv:1205.2875 [hep-ph].
- [40] Jadach, Stanislaw *et al.* *Comput. Phys. Commun.* **64**, 275 (1990). CERN-TH-5856-90.
- [41] S. Frixione, *Phys. Lett. B* **429**, 369 (1998) [hep-ph/9801442].
- [42] J. Pumplin, D. R. Stump, J. Huston, H. L. Lai, P. M. Nadolsky and W. K. Tung, *JHEP* **0207**, 012 (2002) [hep-ph/0201195].
- [43] The ATLAS Collaboration, CERN-OPEN-2008-020.

- [44] G. Bozzi, F. Campanario, M. Rauch, H. Rzehak and D. Zeppenfeld, Phys. Lett. B **696**, 380 (2011) [arXiv:1011.2206 [hep-ph]].
- [45] J. M. Campbell, R. K. Ellis and C. Williams, JHEP **1107**, 018 (2011) [arXiv:1105.0020 [hep-ph]].
- [46] G. Bozzi, F. Campanario, V. Hankele and D. Zeppenfeld, Phys. Rev. D **81**, 094030 (2010) [arXiv:0911.0438 [hep-ph]].
- [47] T. Binoth, G. Ossola, C. G. Papadopoulos and R. Pittau, JHEP **0806**, 082 (2008) [arXiv:0804.0350 [hep-ph]].
- [48] V. Hankele and D. Zeppenfeld, Phys. Lett. B **661**, 103 (2008) [arXiv:0712.3544 [hep-ph]].
- [49] A. Lazopoulos, K. Melnikov and F. J. Petriello, Phys. Rev. D **77**, 034021 (2008) [arXiv:0709.4044 [hep-ph]].
- [50] I. Sahin, J. Phys. **36**, 075007 (2009) [arXiv:0807.4777 [hep-ph]].